JBC RESEARCH ARTICLE

4EBP2-regulated protein translation has a critical role in high-fat diet–induced insulin resistance in hepatocytes

Received for publication, June 28, 2023, and in revised form, September 14, 2023 Published, Papers in Press, October 4, 2023,
https://doi.org/10.1016/j.jbc.2023.105315

Xiao Han[1], Fei Yang[1], Zhengyi Zhang[1], Zhanwu Hou[1], Qiong Sun[1], Tian Su[1], Weiqiang Lv[1], Zhen Wang[1], Chao Yuan[1], Guanfei Zhang[1], Xin Pi[2], Jiangang Long[1,*], and Huadong Liu[2,*]

From the [1]Center for Mitochondrial Biology and Medicine, The Key Laboratory of Biomedical Information Engineering of Ministry of Education, School of Life Science and Technology, Xi'an Jiaotong University, Xi'an, Shaanxi China; [2]School of Health and Life Sciences, University of Health and Rehabilitation Sciences, Qingdao, Shandong China

Reviewed by members of the JBC Editorial Board. Edited by Qi-Qun Tang

A high-fat diet (HFD) plays a critical role in hepatocyte insulin resistance. Numerous models and factors have been proposed to elucidate the mechanism of palmitic acid (PA)-induced insulin resistance. However, proteomic studies of insulin resistance by HFD stimulation are usually performed under insulin conditions, leading to an unclear understanding of how a HFD alone affects hepatocytes. Here, we mapped the phosphorylation rewiring events in PA-stimulated HepG2 cells and found PA decreased the phosphorylation level of the eukaryotic translation initiation factor 4E-binding protein 2 (4EBP2) at S65/T70. Further experiments identified 4EBP2 as a key node of insulin resistance in either HFD mice or PA-treated cells. Reduced 4EBP2 levels increased glucose uptake and insulin sensitivity, whereas the 4EBP2_S65A/T70A mutation exacerbated PA-induced insulin resistance. Additionally, the nascent proteome revealed many glycolysis-related proteins translationally regulated by 4EBP2 such as hexokinase-2, pyruvate kinase PKM, TBC1 domain family member 4, and glucose-6-phosphate 1-dehydrogenase. In summary, we report the critical role of 4EBP2 in regulating HFD-stimulated insulin resistance in hepatocytes.

Insulin resistance is a hallmark of obesity and type 2 diabetes (T2D), wherein peripheral tissues are unresponsive to insulin's hypoglycemic and anabolic properties (1). T2D is commonly associated with weight gain, prolonged inactivity, and/or systemic hyperlipidemia (2, 3), indicating a strong connection between insulin resistance and lipid excess. In the past 2 decades, strong links have been established between organ dysfunction and typical store-neutral lipids in tissues including liver, heart, pancreas, and skeletal muscle (1).

The postprandial rise in plasma insulin triggers hepatic insulin signaling, promotes the conversion of ingested carbohydrates to hepatic glycogen, inhibits endogenous glucose production, and maintains normoglycemia within a narrow range. In patients with T2D, hepatic insulin resistance disrupts these processes, leading to fasting and postprandial hyperglycemia symptoms (4). The deposition of fat in the liver causes nonalcoholic fatty liver disease, which is the most prevalent chronic liver disease worldwide and is closely related to hepatic insulin resistance and T2D (5, 6). Palmitic acid (PA) is one of the most abundant free fatty acids (FFAs) in human plasma, accounting for approximately 30 to 35% of total FFAs. Studies have shown that PA directly impairs insulin signaling in hepatocytes (7, 8). FFAs have many adverse effects, including the promotion of oxidative stress and endoplasmic reticulum stress, activation of protein kinase C, and proinflammatory responses (9).

Proteomic studies of insulin resistance induced by high-fat diet (HFD) stimulation are typically performed under insulin conditions, and there is a lack of research on the effect of HFD itself on hepatocytes. In this study, we used a combination of the phosphorylated proteome and nascent proteome to investigate the mechanism of HFD-induced insulin resistance in hepatocytes. Through the mapping signaling pathways and protein interaction networks, we identified the phosphorylation modification of 4EBP2_S65/T70 as a potential key node for the translation of glycolysis-related proteins in HFD-induced insulin resistance. The mechanistic target of rapamycin complex 1 (mTORC1) is a crucial node that integrates signals from growth factors and nutrients to regulate cell growth and proliferation (10, 11). It regulates protein translation by phosphorylating eukaryotic translation initiation factor 4E-binding proteins (4EBPs) and ribosomal protein S6 kinase (12, 13). The phosphorylation of 4EBPs by mTORC1 prevents eukaryotic translation initiation factor 4E (eIF4E) repression, resulting in increased translation of highly cap-dependent mRNAs (14). One of the three 4EBPs in mammals, 4EBP2, is ubiquitously expressed in fat, liver, and central nervous system (14–16). Recent studies have shown that 4EBPs may have a significant role in regulating lipid metabolism and energy homeostasis (17, 18). For example, in mice treated with 4EBP2 antisense oligonucleotides, increased phosphorylation of RAC serine/threonine-protein kinase (AKT) Ser473 was observed in fat and liver, as well as increased solute carrier family 2, facilitated glucose transporter member 4 (GLUT4) levels in white adipose plasma membrane (18). However, the relationship between HFD-induced insulin resistance and 4EBP2 has not been reported in hepatocytes.

* For correspondence: Huadong Liu, huadongliu@uor.edu.cn; Jiangang Long, jglong@xjtu.edu.cn.

To further explore the mechanism of 4EBP2 in the insulin resistance of hepatocytes, we constructed *Eif4ebp2*$^{TBG\text{-}sh}$ mouse, 4EBP2 knockdown (4EBP2-KD), and mutant cell lines. Our results showed that reducing 4EBP2 level increased glucose uptake and insulin sensitivity, whereas 4EBP2_S65A/T70A mutation exacerbated PA-induced insulin resistance. We also identified the nascent proteome and revealed the glycolysis-related proteins that are translationally regulated by 4EBP2. Therefore, we report the critical role of 4EBP2 in regulating HFD-stimulated insulin resistance in hepatocytes.

Results

Phosphorylated proteomic analysis of PA-stimulated HepG2 cells and HFD mice liver

To investigate the effects of HFD on insulin resistance and to identify key nodes in the hepatic signaling network, we conducted a phosphorylated proteomic analysis of PA-stimulated HepG2 cells and HFD mice liver. First, a well-established HepG2 cell-based model was used to analyze the effects of PA using AKT phosphorylation as an indicator. Consistent with the phenotype of PA-stimulated insulin resistance, attenuated insulin response of AKT (pS473) was observed over time with 300 μM PA (Fig. 1*A*). To explore the progress of signaling network rewiring by PA treatment, HepG2 was cultured for 0, 6, 12, and 24 h with PA, and phosphorylated peptides were enriched for mass spectrometry analysis. Approximately 8900 phosphorylation sites were identified, of which about 5500 phosphorylation sites were available for quantitative analysis. Venn diagram analysis showed that most phosphorylation sites appeared in all samples, with a small number of sites crossing at different time points, whereas a few phosphorylation sites existed independently at discrete time points (Fig. S1*A*). Principal component analysis (PCA) and abundance cluster analysis using heatmaps showed substantial biological repeating and clear differences between groups (Fig. S1, *B* and *C*). A volcano plot was used to determine significant phosphorylation changes following PA stimulation, with cut-off values of |log2 fold change| ≥ 1 and p-value < 0.05 (Figs. 1*B* and S1*D*). Kyoto Encyclopedia of Genes and Genomes analysis of proteins with changes in phosphorylation revealed significant involvement with the mTOR pathway (Fig. 1*C*), which has a well-established role in metabolism, and phosphorylation of 4EBP2_S65/T70 was most significantly changed in the downstream of mTOR. Interestingly, the most significant pathway is the proteoglycans in cancer. The synthesis and metabolism of proteoglycans were regulated by energy metabolism (19). For example, SDC1 and PDCD4 are involved in tumor growth (20, 21). Our data showed that the phosphorylation of SDC1_S285 and PDCD4_S94 increased after PA. Different patterns of change during PA treatment were observed. For example, phosphorylation of SIK2_S587 increased immediately, whereas Cdc42-interacting protein 4 (TRIP10)_pS298 level decreased. Many phosphorylation sites showed dramatic fluctuations.

Second, we also carried out phosphorylated proteome analysis on the livers of HFD mice. PCA showed substantial biological repeating and clear differences within groups. The heatmap for the abundance cluster analysis indicated the data quality (Fig. S2, *A* and *B*). A volcano plot was used to determine significant phosphorylation changes following HFD, with the cut-off values of ΔZ-Score ≥ 1 and p-value < 0.05 (Fig. 1*E*). Based on pathway enrichment of differentially phosphorylated proteins, we found that insulin signaling and mTOR signaling were prominent, consistent with the PA proteome results (Fig. S2*C*). Phosphorylation of 4EBP2_T70, 4EBP2_T37/T46, RPTOR_S863, RPTOR_S722, and mTOR_S1261 was decreased (Fig. 1*F*). Overall, our results suggest that 4EBP2 plays a critical role in regulating HFD-stimulated insulin resistance in hepatocytes and highlight the importance of mTOR signaling in metabolism.

PA induces rewiring of phosphorylation signaling in insulin pathway

Upon PA stimulation, we observed significant changes in phosphorylation modifications at multiple sites in proteins involved in the insulin signaling pathway, as shown in Figures 2 and S3. The phosphorylation of SLC2A4/GLUT4-related proteins was altered in both the PA-induced and the HFD-induced phosphorylated proteome. Additionally, the phosphorylation of TBC1 domain family member 4 (TBC1D4), TRIP10, and protein transport protein Sec16A (SEC16A) was significantly changed following PA stimulation (Fig. 2), while DENND4C and SEC16A showed phosphorylation changes in HFD mice (Fig. S2*D*). TBC1D4 and TRIP10 are downstream of the insulin signaling pathway and promote insulin-induced translocation of glucose transporter SLC2A4/GLUT4 to the plasma membrane, increasing glucose uptake (22–25). The phosphorylation of TBC1D4_S588, commonly observed in T2D (26), was increased by PA stimulation (Fig. 1*D*), possibly inducing cellular endocytosis (27) and demonstrating the reliability of the data. The phosphorylation of TRIP10_S289 was significantly decreased during PA stimulation, which may regulate glucose uptake. SEC16A, which can regulate the transport of GLUT proteins (28), also showed changes in its phosphorylation levels in both PA-treated and HFD mice.

Furthermore, we observed many known phosphorylation changes in proteins involved in the insulin signaling pathway, such as serine/threonine-protein kinase SIK2 (SIK2), a kinase of IRS1_S794 that regulates the pathway (29). The phosphorylation of S587 reduces SIK2 activity (30). We observed an increase in SIK2_pS587 levels, indicating that SIK2 may be involved in PA-stimulated inhibition of the insulin signaling pathway. An increase in PRKCA_pS226 was also observed, which has been reported to induce enzymatic activity (31–33). Additionally, several proteins related to fatty acid metabolism, including fatty acid synthase, acetyl-coenzyme A synthetase, cytoplasmic, and diacylglycerol O-acyltransferase 1, underwent phosphorylation fluctuations at different stages of PA treatment. Of note, we observed a reduction in the phosphorylation of mTORC1-regulated mRNA translation axis proteins, including RPTOR_pS863, RPTOR_pS722, mTOR_pS1261, and 4EBP2_pS65/pT70, which is consistent with a report that

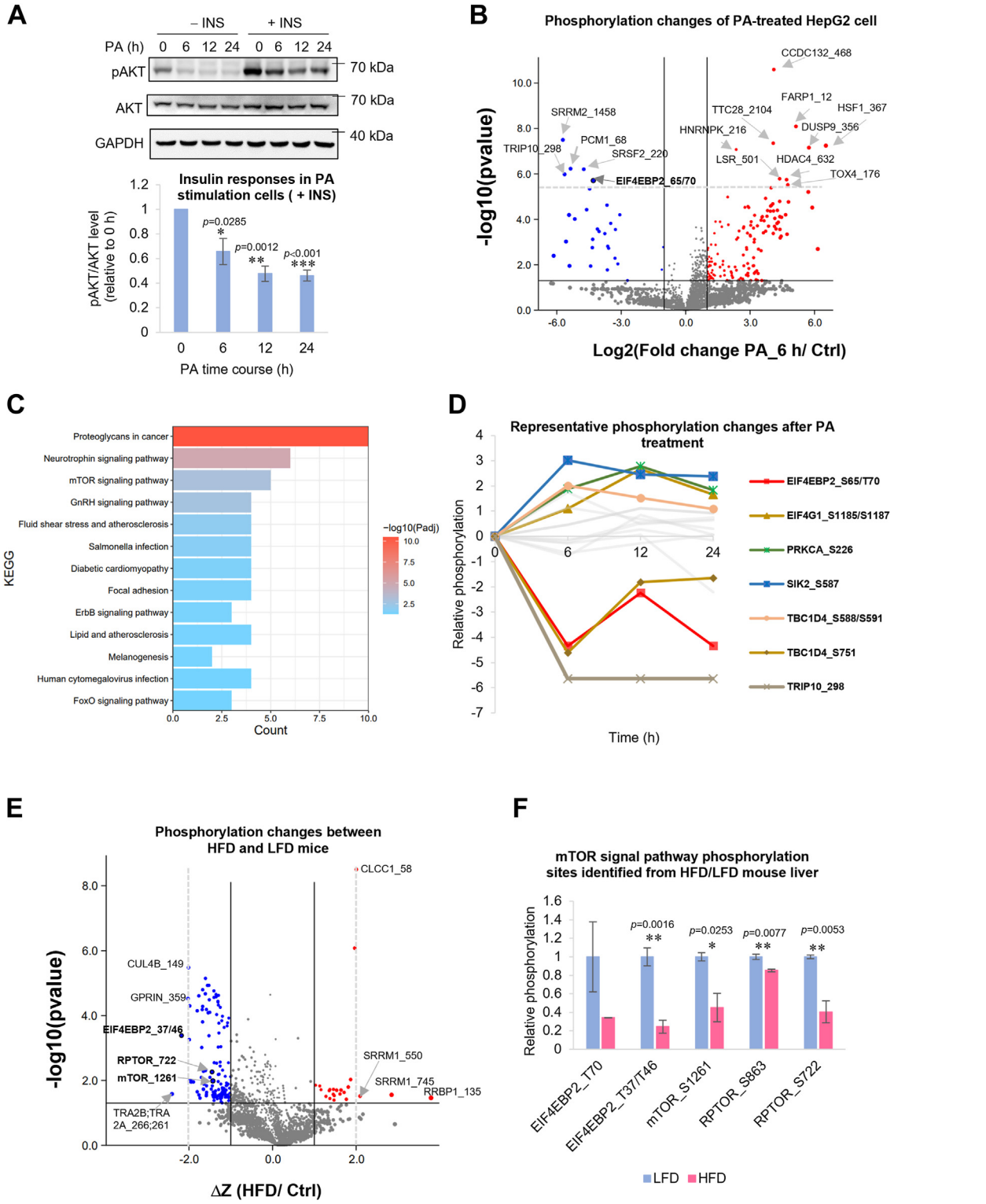

Figure 1. Phosphorylated proteomics analysis of PA-stimulated HepG2 cells and HFD mice liver. *A*, Western blot of Akt phosphorylation (S473) after insulin (INS) stimulation in the presence of PA. Cells were treated with PA (300 μM) for 0, 6, 12, or 24 h before being stimulated with or without 100 nmol/l insulin for 10 min n = 3 biologically independent samples. *B*, volcano analysis of phosphorylated peptides from HepG2 cells stimulated by PA for 6 h or controls. Phosphorylation sites with *p*-value < 0.05 are present above the *horizontal lines* (*gray*). Phosphorylation sites with significant fold-change are outside the *gray vertical lines* (log2-fold change ≥ 1, *p*-value < 0.05, *red*; log2 fold change ≤ −1, *p*-value < 0.05, *blue*; n = 3 biologically independent samples). *C*, KEGG enrichment analysis of phosphorylation sites with significant difference (PA *versus* control, cut-off at |log2-fold change| ≥ 2 and *p*-value < 0.05). *D*, representative rewiring progresses of phosphorylation sites with significant changes in insulin signaling pathway. *E*, volcano analysis for phosphorylated sites from HFD and LFD mice liver (n = 4). *F*, relative changes of phosphorylation sites with in mTOR signaling pathway. *0.01 < *p* < 0.05, **0.001 < *p* < 0.01, ***$p < 0.001$. HFD, high-fat diet; KEGG, Kyoto Encyclopedia of Genes and Genomes; PA, palmitic acid.

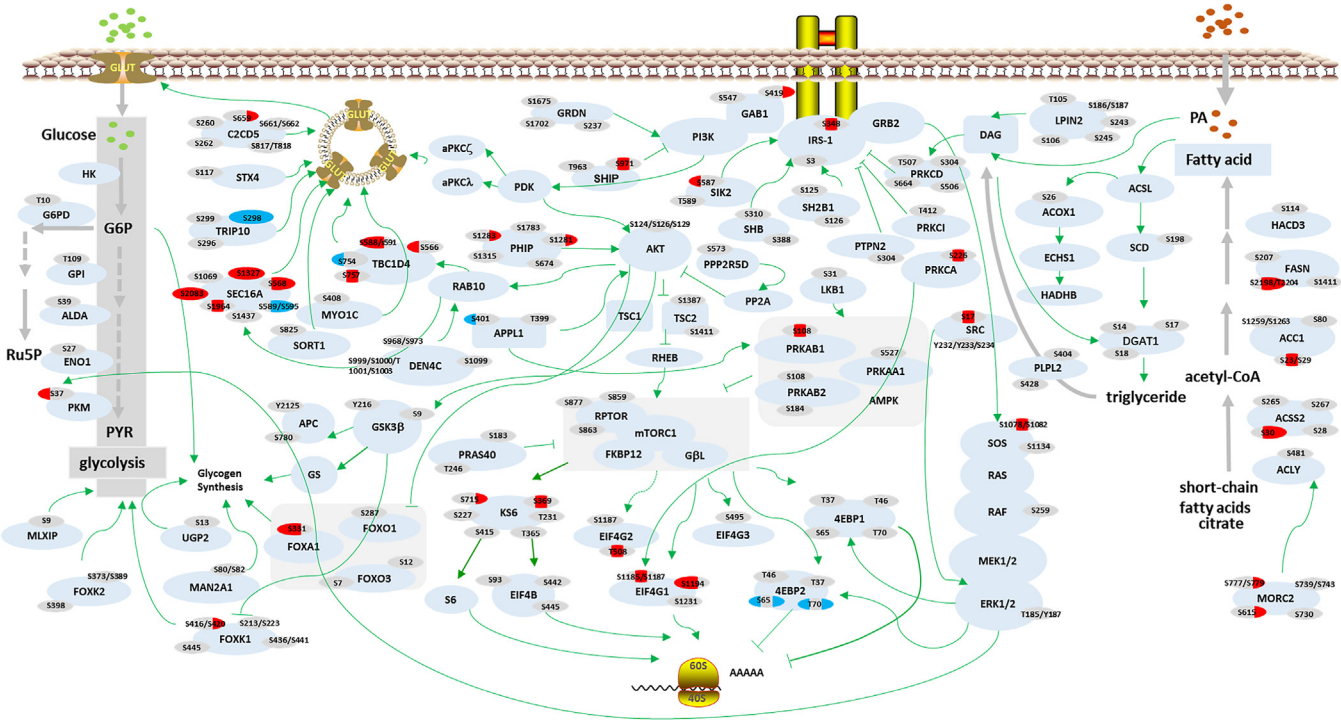

Figure 2. Insulin signal pathway. Interaction network of insulin signaling pathway showing significantly changed phosphorylation events with PA stimulation. Each of the phosphorylation site was labeled with three color codes (*left*, 6 h; *middle*, 12 h; *right*, 24 h). The site with no significant change was marked by *gray*. The significantly changed site was marked by *red* for upregulated or by *blue* for downregulated. The cut-off was set as |log2 fold change| ≥ 1, *p*-value < 0.05. PA, palmitic acid.

HFD inhibited mTORC1 activity (34). Notably, the phosphorylation of 4EBP2 changes were considerable in cell lines and mice livers. The phosphorylation of 4EBP2_S65/T70 was decreased throughout PA stimulation, making the protein more available to bind eIF4E in competition with eIF4G and subsequently inhibit protein translation (35, 36). These findings were considerable in cell lines and mice livers. While the roles of some of the observed phosphorylation changes in well-known insulin-responding proteins have not been documented, our results provide new insights into the effect of PA on the phosphorylation signaling of the insulin pathway, inducing rewiring of the pathway.

4EBP2-KD increases glucose uptake and improves insulin sensitivity

We knocked down 4EBP2 in hepatocytes to obtain 4EBP2-KD cell lines and determine its regulatory role in glucose uptake and insulin signaling pathway. Cell growth was not affected after 4EBP2-KD (Fig. 3*A*), consistent with previous reports. We then tested insulin-regulated glucose uptake and found that glucose uptake was decreased after 6 h PA treatment in wildtype cells (Fig. 3*B*). However, 4EBP2-KD cell lines showed dramatically improved glucose uptake. To validate our findings in an *in vivo* model, we employed an AAV virus to knocked down 4EBP2 in mice liver, resulting the generation of *Eif4ebp2*$^{TBG\text{-}sh}$ mice. The expression of 4EBP2 protein in the mice liver was analyzed through immunohistochemical (Fig. 3*C*), Western blot, and RT-PCR (Figs. 3*E* and S4*A*), confirming the successful knockdown effect of 4EBP2. Importantly, the reduction of 4EBP2 had no effect on the liver function as assessed by H&E section staining and liver function test, including AST and ALT (Figs. 3*C* and S4*B*). However, the *Eif4ebp2*$^{TBG\text{-}sh}$ mice showed increased sensitivity to insulin compared with the control group (Fig. 3*D*). To further understand the molecular mechanism underlying this effect, we detected insulin-responding marker AKT. Although the protein levels were similar, Western blot bands of AKT(pS473) were increased in *Eif4ebp2*$^{TBG\text{-}sh}$ mice livers compared with controls (Fig. 3*E*). The same trends were observed in hepatocytes, as shown in Figures 3, *F–G* and S4, *C–E*. Collectively, our data indicate that 4EBP2 is involved in PA response, glucose uptake, and insulin signaling regulation and that its knockdown leads to increased glucose uptake and improved insulin sensitivity.

Nascent proteomics changes caused by PA-stimulated insulin resistance

We aimed to investigate the effects of PA-stimulated insulin resistance on nascent proteomics changes using an AHA labeling technique commonly used to probe changes in protein translation (37, 38). Phosphorylation proteome analysis indicated that protein translation regulation was involved in PA treatment. As shown in Figure 4*A*, AHA was used to substitute Met in the medium to label nascent proteins in HepG2 cells. Labeled proteins were coupled with alkynyl–biotin through click chemistry reaction, followed by NeutrAvidin bead enrichment and mass spectrum quantification. AHA labeling and the click chemistry reaction were detected successfully by

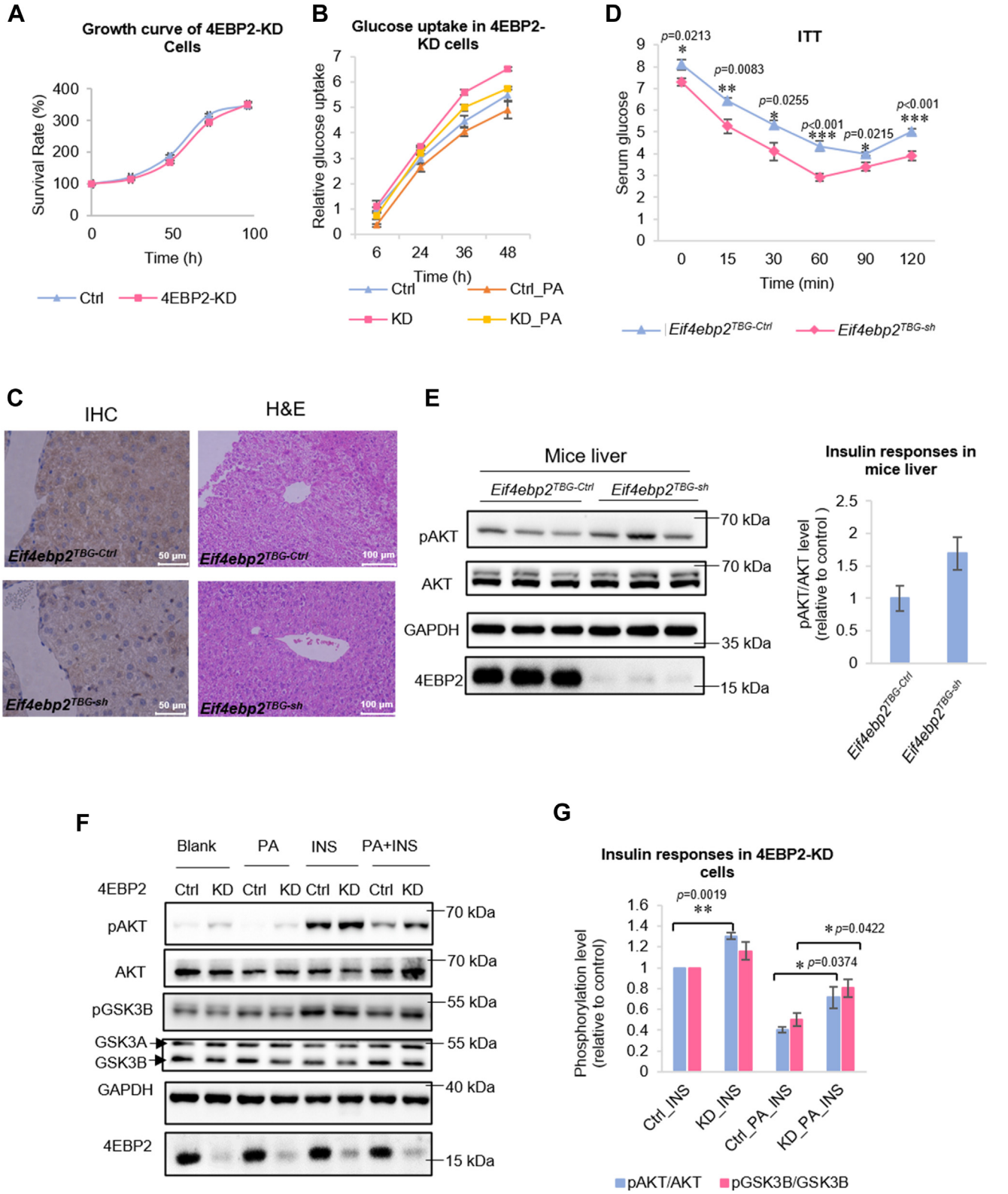

Figure 3. 4EBP2-KD response to insulin. *A*, the growth curve of 4EBP2-KD or control HepG2 cells (n = 4 biologically independent samples). *B*, the glucose uptake assay of 4EBP2-KD or control HepG2 cells (n = 3 biologically independent samples). *C*, 4EBP2 immunohistochemistry (IHC) and H&E section staining of *Eif4ebp2*$^{TBG-sh}$ or control mice liver. *D*, the insulin tolerance test (ITT) of *Eif4ebp2*$^{TBG-sh}$ or control mice (n = 8 biologically independent animals). *E*, Western blot analysis of AKT (pS473) in live of 4EBP2-KD or control mice. *F*, Western blot analysis of AKT (pS473) and GSK3B (pS9) levels in 4EBP2-KD or control AML12 cells in response to insulin (n = 3 biologically independent samples). *G*, statistical analysis of AKT (pS473) and GSK3B (pS9) levels in 4EBP2-KD or control AML12 cells in response to insulin. 4EBP2-KD, 4EBP2 knockdown; 4EBP2, eukaryotic translation initiation factor 4E-binding protein 2; AKT, RAC serine/threonine-protein kinase; GSK3B, glycogen synthase kinase-3 beta.

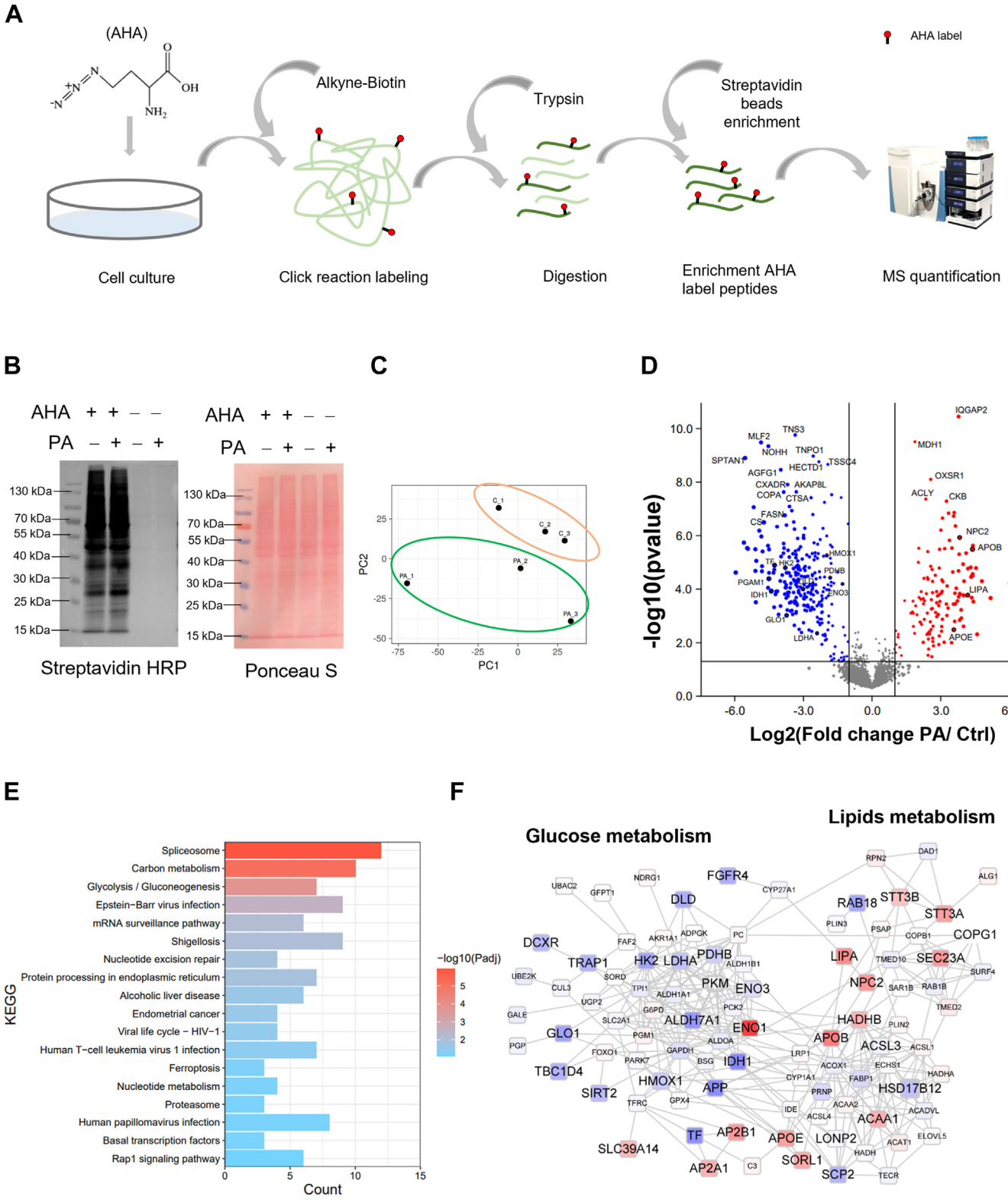

Figure 4. Nascent proteome analysis. *A*, schematic diagram of AHA-labeled nascent proteome detection. *B*, Western blot assay of biotin-labeled nascent proteins by click reaction. *C*, principal component analysis of quantified nascent peptides from PA-treated or control cells (n = 3 biologically independent samples). *D*, volcano analysis of identified nascent proteins from PA-treated or control cells (n = 3 biologically independent samples). *E*, KEGG pathway enrichment analysis of decreased nascent proteins after PA stimulation of HepG2. The cut-off was set as log2 fold change ≤ −1 and *p*-value < 0.05 (n = 3 biologically independent samples). *F*, analysis of PPI network between glucose and fatty acid metabolism–related proteins. The *blue nodes* represent the decreased nascent proteins by PA treatment. The *red nodes* represent the increased nascent proteins by PA treatment. The smaller of the *p*-value, the larger of the font (n = 3 biologically independent samples). 4EBP2, eukaryotic translation initiation factor 4E-binding protein 2; 4EBP2-KD, 4EBP2 knockdown; KEGG, Kyoto Encyclopedia of Genes and Genomes; PA, palmitic acid.

Western blotting (Fig. 4*B*). Approximately 4500 AHA-labeled sites from about 2000 proteins were characterized in HepG2 cells with or without PA treatment. As shown in Figure 4*C*, PCA analysis showed biological repeatability and clear differences within groups. A volcano plot was used to determine significant changes in nascent proteins upon PA stimulation, with cut-off values of |log2 fold change| ≥ 1 and p-value < 0.05 (Fig. 4*D*). As reduced 4EBP2 phosphorylation leads to translation inhibition, decreased nascent proteins after PA stimulation were analyzed by Kyoto Encyclopedia of Genes and Genomes and GO pathway enrichment. Pathway enrichment analysis revealed that PA treatment caused the rearrangement of glucose and lipid metabolism, with significant changes observed in carbon metabolism, glycolysis/gluconeogenesis, and cellular catabolic process pathways (Figs. 4*E* and S5*A*). As shown in Figure 4*F*, glucose metabolism–related proteins including hexokinase-2 (HK2), pyruvate kinase PKM (PKM), TBC1D4, and L-xylulose reductase were significantly reduced, while apolipoprotein B-100, apolipoprotein E, and lysosomal acid lipase/cholesteryl ester hydrolase were increased. The reduced nascent proteins indicated that PA inhibited glycolysis, resulting in insulin resistance, while the increased nascent proteins could be attributed to elevated concentrations of cellular fatty acids. Additionally, after PA stimulation, we analyzed increased nascent proteins and discovered that the cholesterol metabolism pathway held significant importance (Fig. S5*B*). All these findings suggest that PA-stimulated insulin resistance leads to significant changes in nascent proteomics related to glucose and lipid metabolism.

4EBP2 regulates the translation of glycolysis proteins and modulates glucose uptake

To confirm the protein changes identified by nascent mass spectrometry, Western blotting was conducted to check the expression levels of glucose metabolism–related proteins (Fig. 5*A*). The results showed that HK2 level was significantly decreased by PA treatment, consistent with the results of the nascent proteomics analysis. Additionally, HK2 was significantly upregulated in 4EBP2-KD cells, confirming the direct regulation between 4EBP2 and HK2 (Figs. 5*A* and S6*A*). Other key proteins involved in glucose metabolism, including GLUT4, PKM, and glucose-6-phosphate 1-dehydrogenase (G6PD), were also investigated in *Eif4ebp2*$^{TBG\text{-}sh}$ mice livers (Fig. S6*B*). Similarly, PKM and G6PD were found to be increased in 4EBP2-KD cells, regardless of whether the cells had undergone PA treatment or not (Fig. 5*A*). To determine whether the changes of these proteins were translationally regulated, nascent proteins were labeled with alkynyl biotin and subsequently enriched using NeutrAvidin beads. Nascent proteome analysis showed that 4EBP2-KD increased the protein synthesis of HK2, PKM, G6PD family proteins, and others (Fig. 5*B*). Western blot detection confirmed that nascent HK2, G6PD, and PKM were significantly increased in 4EBP2-KD HepG2 cells (Fig. 5*C*). Interestingly, the mRNA levels of HK2, G6PD, and PKM were not changed (Fig. S6*C*). In addition, we isolated ribosome-binding mRNA and total mRNA from *Eif4ebp2*$^{TBG\text{-}sh}$ mice livers and 4EBP2-KD cells and carried out real-time quantitative polymerase chain reaction. The results showed significant increases in levels of various ribosome-binding mRNAs, such as *Hk*, *Pkm*, *G6pd*, *Pfkl*, *Aldoa*, *Aldob*, and *Tbc1d4* (Fig. 5*D*). However, in 4EBP2-KD cells, *Pkm* and *Eno1* showed an increase, while the total mRNA almost unchanged (Fig. S6, *C* and *D*). These findings confirm that the translation of these proteins is regulated by 4EBP2.

To investigate whether 4EBP2-regulated proteins are involved in glucose metabolism, glucose and its analog 2-Deoxy-D-glucose (2-DG) were used to check phosphorylation markers in the insulin pathway. As shown in Figure 5*E*, 4EBP2-KD cells showed increased levels of phosphorylation markers pAKT and pGSK3B in high-glucose medium. However, 4EBP2 showed a very moderate regulatory function in 2-DG medium. All these data indicate that the mechanism by which 4EBP2-KD boosted pAKT levels is glucose metabolism specific. Furthermore, we checked whether 4EBP2-KD affected glucose uptake. As shown in Figure 5*F*, glucose uptake of all cells was reduced by both PA and 2-DG. However, 4EBP2-KD cells showed a greater rescue of glucose uptake by 2-DG. When the glucose uptake inhibitor phloretin was added, the levels of insulin markers such as pAKT or pGSK3B in 4EBP2-KD cells were dramatically reduced (Fig. 5*G*). Taken together, the results of the 2-DG and phloretin experiments indicate that 4EBP2 regulates insulin-induced glucose uptake.

4EBP2-S65A/T70A mutation dispelled insulin sensitization

There are two well-documented critical phosphorylation regions for the regulatory function of 4EBP2 (39). Our phospho-proteome data revealed that PA induced the inhibitory activity of 4EBP2 by decreasing the phosphorylation at S65/T70 instead of T37/T46. To verify the regulation sites, stable cell lines were constructed that overexpressed 4EBP2 (OE), 4EBP2_T37A/T46A (MUT1), and 4EBP2_S65A/T70A (MUT2). As shown in Figure 6*A*, similar pAKT levels were observed in all three 4EBP2-overexpressing cell types upon insulin stimulation. However, PA treatment failed to induce pAKT reduction in the OE and MUT1 cell lines. Only MUT2 cells showed sensitivity to PA treatment compared with control cells (Fig. 6*A*). Consistently, similar results were observed for pGSK3B levels. All these data indicate that the S65/T70 region is critical for proper 4EBP2 function. However, 4EBP2-OE stable cell lines did not show the opposite phenotypes of knockdown cell lines. Unchanged glucose uptake in 4EBP2-OE cells provided further evidence that stable cell lines might adapt to excessive 4EBP2 levels by changing its efficiency (Fig. 6*B*). By overexpressing wildtype 4EBP2, MUT1, and MUT2 plasmids in 4EBP2-KD cells, we found that the increased pATK or pGSK3B levels of 4EBP2-KD cells were decreased by MUT2 but not by wildtype 4EBP2 or MUT1 (Fig. 6*C*). More importantly, consistent with our nascent proteomics data, HK2 levels were also reduced in MUT2 cells (Fig. 6*C*). At the same time, we quantified the ribosome-bounding mRNA in MUT2 cells and found significant reduction in *Hk1*, *Pfkl*, *G6pd2*, and *Aldob* compared to control groups (Fig. 6*D*). Taken together, these

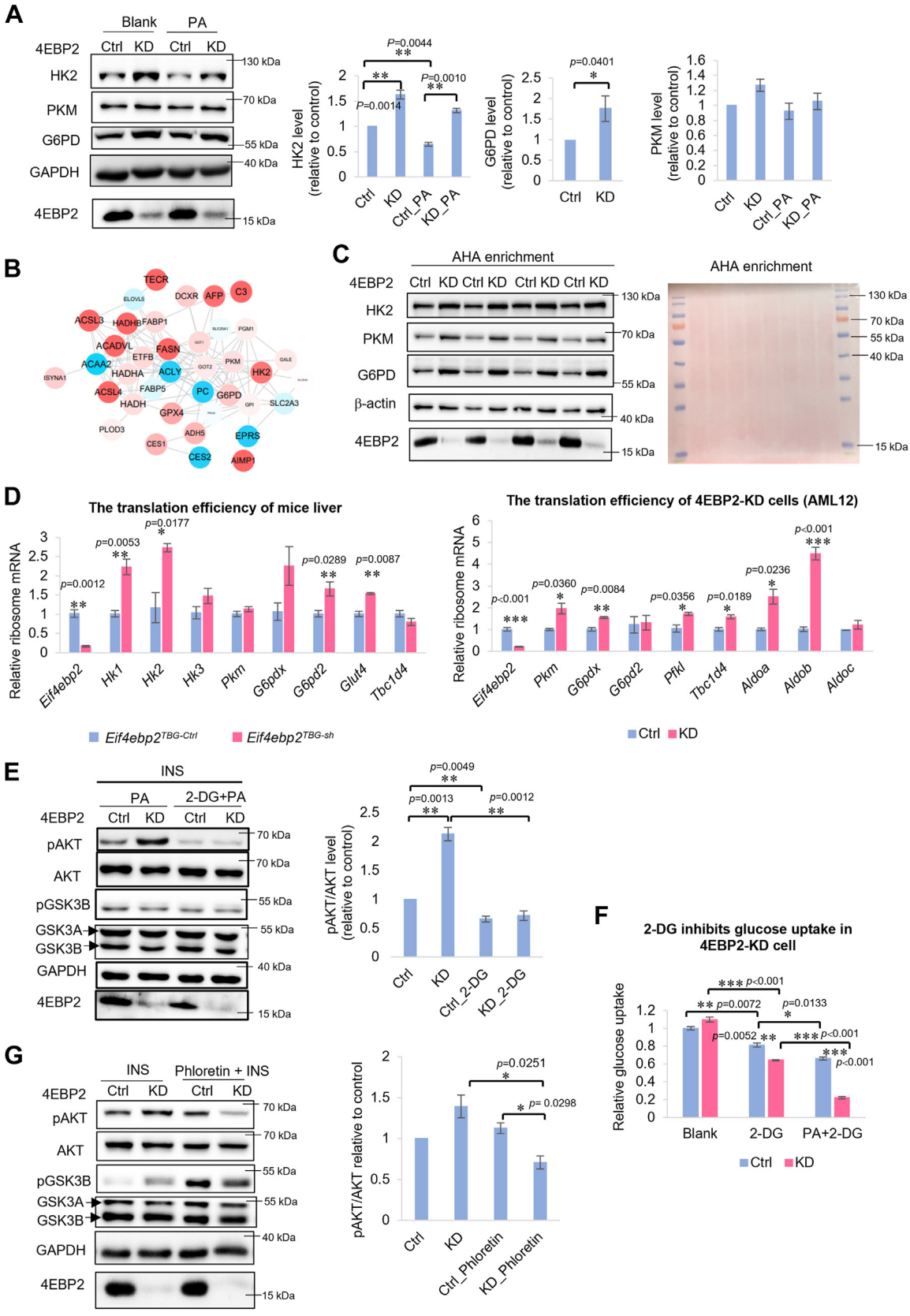

Figure 5. 4EBP2 govern the translation of glucose metabolism–related proteins. *A*, the Western blot assay of glucose metabolism–related proteins in 4EBP2-KD and control HepG2 cells with/without PA treatment (n = 3 biologically independent samples). *B*, the nascent level changes of glucose metabolism–related proteins of 4EBP2-KD and control HepG2 cells (n = 2 biologically independent samples). *C*, the Western blot assay of biotin-labeled nascent proteins by click reaction in 4EBP-KD cell (n = 4 biologically independent samples). *D*, quantitative analysis of ribosomal binding mRNA by RT-PCR (n = 3 biologically independent samples). *E*, the Western blot of insulin-responding proteins in 4EBP2-KD and control cell lines with/without 2-DG

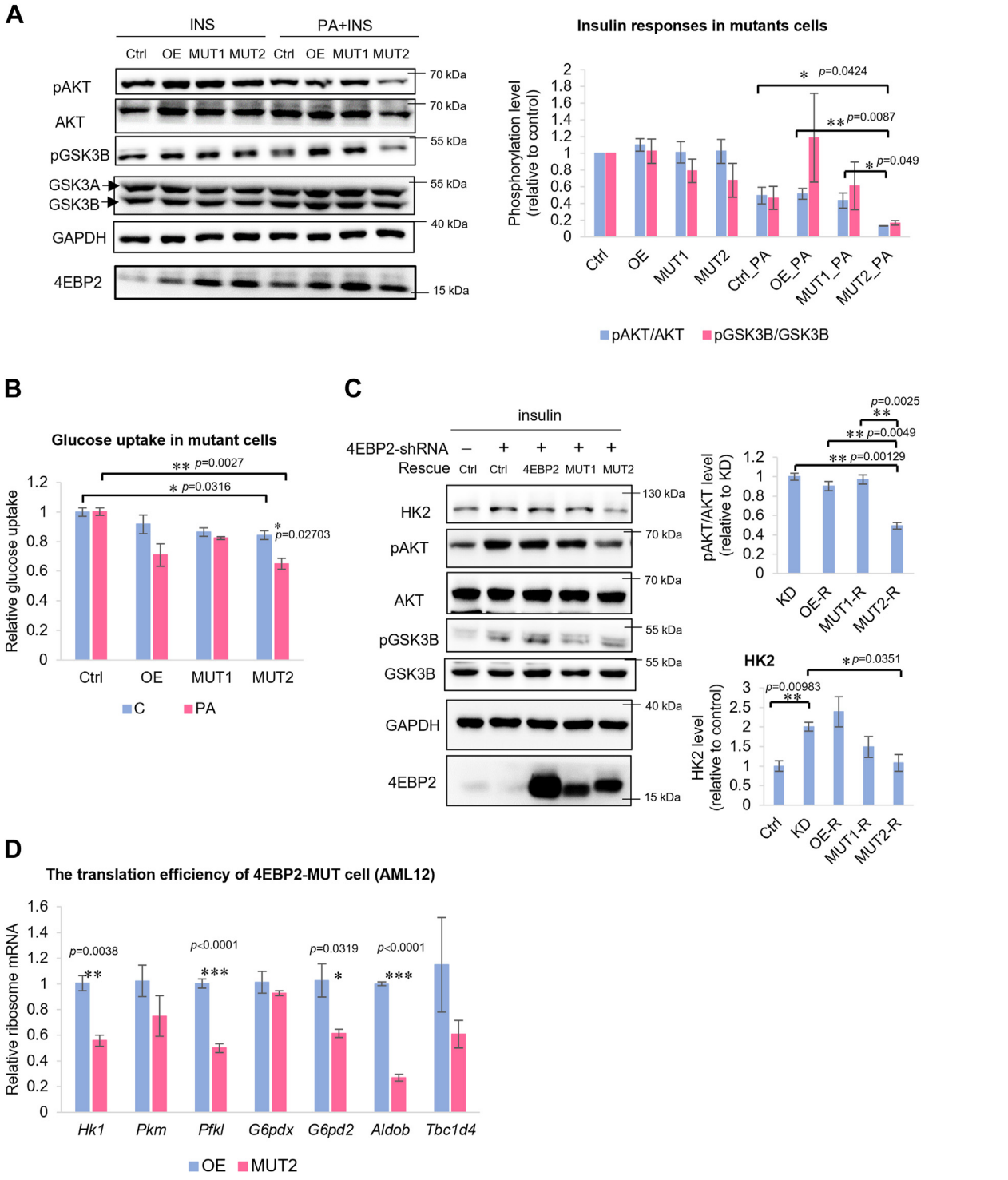

Figure 6. Insulin sensitivity assay of cells overexpressing 4EBP2 mutants. *A*, the Western blot assay of AKT (pS473) and GSK3B (pS9) in cells overexpressing different 4EBP2 mutants (n = 3 biologically independent samples). *B*, the glucose uptake assay of cells overexpressing different 4EBP2 mutants with/without PA (n = 3 biologically independent samples). *C*, the rescue assay of 4EBP2 mutants in 4EBP2-KD HepG2 cells (n = 3 biologically independent samples). *D*, quantitative analysis of ribosomal binding mRNA by RT-PCR (n = 3 biologically independent samples). 4EBP2, Eukaryotic translation initiation factor 4E-binding protein 2; 4EBP2-KD, 4EBP2 knockdown; AKT, RAC serine/threonine-protein kinase; GSK3B, Glycogen synthase kinase-3 beta; HK2, hexokinase-2.

(n = 3 biologically independent samples). *F*, glucose uptake analysis of 4EBP2-KD and control cells with/without 2-DG. *G*, 4EBP2-KD and control cell lines response to insulin with phloretin. Western blot analysis of AKT (pS473) and GSK3B (pS9) levels (n = 3 biologically independent samples). 4EBP2, eukaryotic translation initiation factor 4E-binding protein 2; 4EBP2-KD, 4EBP2 knockdown; AKT, RAC serine/threonine-protein kinase; GSK3B, glycogen synthase kinase-3 beta; HK2, hexokinase-2; PA, palmitic acid; PKM, pyruvate kinase PKM.

results show that phosphorylation of the 4EBP2_S65/T70 region is responsible for PA-induced insulin resistance *via* regulation of the translation of hexokinase, PKM, G6PD, and TBC1D4 and glucose uptake.

Discussion

The link between HFD and insulin resistance is well-established, as HFD leads to increased levels of PA in both plasma and liver. PA is commonly used to stimulate HepG2 cells in studies investigating the effects of HFD on the liver at a cellular level. The intracellular levels of PA exceed mitochondrial oxidation and are converted to harmful lipids like diacylglycerols, and ceramides ultimately leads to cellular damage and insulin resistance through increased reactive oxygen species and mitochondrial stress (40). Numerous models have been proposed to understand the mechanism of PA-induced insulin resistance, but the complexity of cellular responses to PA has made it difficult to identify a clear pathway. Despite this, systematic proteomics research on the effects of PA stimulation on hepatocytes has been lacking, particularly regarding how cells respond to PA-stimulated signal transduction, which is typically obtained through phosphorylation signals. To fill this gap, we conducted a study on the phosphorylation proteomics of different stages of PA-stimulation HepG2 cells and statistically analyzed the changes in signal transduction pathways. Taking advantage of the simplified environmental factors in cell line systems, we systematically characterized the dynamic phosphorylation changes within the metabolic network. We were particularly interested in the early responses and significant changes in 4EBP2 phosphorylation, which were confirmed in the livers of HFD mice. While 4EBP2 has been reported to play an important role in lipid metabolism and insulin resistance, the regulatory role of 4EBP2 under PA stimulation has not been documented. Our data demonstrate that 4EBP2 plays a critical part in insulin resistance by bridging PA stimulation and protein translational regulation. We found that 4EBP2-KD rescued PA-induced reductions in pAKT or pGSK3B levels, as well as PA-induced reductions in glucose uptake in response to insulin treatment.

The 4EBP2 protein is key factor in regulating cap-dependent translation downstream of the insulin signaling pathway. The folded state of phosphorylated 4EBP2_T37/T46 was weakly stable, causing a 100-fold reduction in affinity with EIF4E, whereas fully phosphorylated 4EBP2 was more folded, with an approximately 4000-fold reduction in affinity (36). Phosphorylation-induced folding stability is a key mechanism of phosphorylation regulation of the 4EBP–EIF4E interaction. Phosphorylation may lead to electrostatic repulsion at the negative surface of EIF4E, or S65 phosphorylation may inhibit binding by disrupting the helical structure of the YXXXXLW motif (41, 42). Our phosphorylated proteome data showed that PA treatment reduced the phosphorylation of 4EBP2_S65/T70, leading us to speculate that the PA might decrease the translation of metabolism-related proteins involved in insulin distal signaling by reducing S65/T70 phosphorylation. Using a nascent proteome enrichment strategy, we identified 4EBP2 regulating proteins. Many key metabolic proteins, such as HK and PKM and G6PD, were significantly altered by 4EBP2-KD or mutations during PA treatment. For instance, PA treatment reduced the protein level or nascent level of HK2, potentially through the activation of 4EBP2's inhibitory function. Knockdown of 4EBP2 rescued HK2 expression, and while overexpression of wild-type 4EBP2 failed to decrease HK2 levels, phosphorylation-defective mutant 4EBP2_S65A/T70A achieved this aim. Additionally, we assessed the translation level of glycolysis-related proteins in *Eif4ebp2*$^{TBG\text{-}sh}$ mice liver, AML12, and HepG2 4EBP2-KD cells and found a consistent overall trend of increased translation, although differences were observed.

Elucidating the whole mechanism still requires filling in many missing pieces of the puzzle. The relationship between 4EBP2 phosphorylation and pATK is a complex maze. Insulin signaling leads to phosphorylation of AKT by mTORC2, which in turn activates mTORC1 and phosphorylates 4EBP2 (43–46), resulting in increased translation of metabolic proteins (46). Surprisingly, our nascent proteome revealed that 4EBP2 dysfunction caused a decrease in translation of many proteins, including PC and ACLY. These proteins maybe involved in a feedback loop that involves elevated pATK levels, but the specifics of this loop are still unknown. Additionally, 4EBP2 may regulate glucose uptake, leading to activation of AKT and increased pAKT levels. Our experiments using a glucose analog indicate that 4EBP2 does indeed regulate glucose uptake. Although some possibilities remain unconfirmed, our data strongly suggest that targeting 4EBP2 could be an effective means of restoring insulin resistance induced by HFD in hepatic cells.

In summary, as shown in Figure 7, this study provides novel data that show the key role of 4EBP2_S65/T70 in insulin resistance in hepatic cells. The effects of palmitate on hepatic

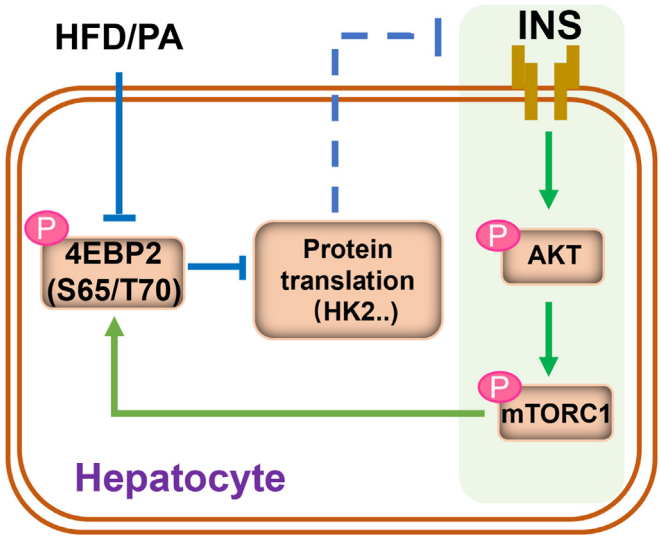

Figure 7. Proposed mechanisms of PA/HFD-induced insulin resistance in hepatocytes. PA/HFD decreased the phosphorylation of 4EBP2_S65/T70 significantly, which inhibited the translation of glucose metabolism related proteins, such as HK2, PKM, etc, and produced insulin resistance. 4EBP2, eukaryotic translation initiation factor 4E-binding protein 2; HFD, high-fat diet; HK2, hexokinase-2; PA, palmitic acid; PKM, pyruvate kinase PKM.

insulin resistance are mediated by inhibition glycolysis-related proteins translation through decreased the phosphorylation of 4EBP2_S65/T70.

Experimental procedures

Animal and diets

All animal protocols were approved by the Animal Care and Use Committee of the School of Life Science and Technology, Xi'an Jiaotong University. Male C57BL/6 mice, 5 weeks old, were fed ad libitum and housed in a temperature-controlled environment (23 ± 2°C) with a 12/12-h light/dark cycle. Mice were maintained with either a normal chow diet (10% kcal% fat; catalog no. D12450; Research Diet) or a high-fat diet (60% kcal% fat; catalog no. D12492; Research Diet) for 12 weeks.

Mice liver 4EBP2 knockdown and insulin tolerance test

AAV virus (HBAAV2/8-TBG-Mir30-m-Eif4ebp2-ZsGreen and HBAAV2/8-TBG-ZsGreen) were purchased from Han-Bio Technology, (mouse *Eif4ebp2* shRNA: 5′-CACGAAT-CATTTATGACCGAA-3′). 7-week-old male mouse were injected with 100 μl (1*10^12 vg/ml) virus through tail vein, and the expression of 4EBP2 decreased after 4 weeks and successfully constructed $Eif4ebp2^{TBG\text{-}sh}$ mouse.

Firstly, $Eif4ebp2^{TBG\text{-}sh}$ (n = 8) and $Eif4ebp2^{TBG\text{-}Ctrl}$ (n = 8) mice were starved for 6 h. Secondly, 0.05 U/ml insulin (P3375, Beyotime Biotechnology) solution was prepared with normal saline, then injected intraperitoneally at the dosage of 0.5 U/kg. Finally, the blood glucose was measured for 0, 15, 30, 60, 90 and 120 min.

Cell culture

Cell lines (HEK293T; HepG2; LO2) were cultured in Dulbecco's modified Eagle's medium (DMEM) containing high glucose (12100061, Thermo Fisher) supplemented with 10% fetal bovine serum (FBS); AML12 was cultured in DMEM/F12 (1320033, Thermo Fisher) supplemented with 10% FBS, 1% ITS Liquid Media (0341, Beyotime Biotechnology), and dexamethasone (408850, Aladdin) 40 ng/ml and all mediums with 100 U/ml penicillin and 100 μg/ml streptomycin (T488, Beyotime Biotechnology).

The preparation of the PA solution

The preparation of the PA solution was carried out according to the following protocol (47): First, buffer A was created by mixing 30% 0.1 M NaOH with 70% ethanol in a well-distributed manner. Subsequently, buffer B was formulated by combining 10% fatty acid-free BSA in H-DMEM without FBS. Buffer C was prepared by dissolving 200 mM sodium palmitate in buffer A, ensuring complete dissolution at 95 °C. To create the PA solution (5 mM), 2.5% of buffer C was dissolved in buffer B and thoroughly mixed. This mixture was then subjected to a 37 °C water bath for 4 h, maintaining a pH of 7.4, and filtered through a 0.22 μm microporous membrane to obtain the final PA solution, which was subsequently stored at −20 °C for future use.

In vitro *models of insulin resistance*

HepG2 cells are commonly used to study liver insulin resistance *in vitro*. PA (P9767, Sigma) as a common saturated fatty acid, is commonly used to construct insulin-resistance models. A total of four time-course sample sets of HepG2 cell with PA were analyzed and described in Results. Each sample set comprised of three biological replicates. The time course of PA (300 μM) includes 0, 6, 12, and 24 h in H-DMEM with 10% FBS. After PA stimulation, cells were initially starved for 4 h before being stimulated with insulin for 10 min in preparation for the Western blot analysis of AKT phosphorylation. Following this, they were gently washed with pre-cooled PBS and promptly harvested on ice. All cells incubated at 37 °C in a humidified atmosphere with 5% CO_2.

Recombinant plasmids and transfection

The target sequence of the human EIF4EBP2 shRNA plasmid was 5′-CTCGAATCATTTATGACAGAA-3′, mouse *Eif4ebp2* shRNA was 5′-CACGAATCATTTATGACCGAA-3′. 4EBP2_T37A/T46A and S65A/T70A were synthesized by Tsingke Biotechnology. To generate a stable strain, HEK 239T cells were transformed with an overexpression plasmid (TK-PCDH-copGFP-T2A-Puro), a knockdown plasmid (pLKO1) respectively to produce lentivirus. Collect culture medium to infect HepG2, AML12, and LO2 cells for 48 h. The infected cells were seeded in medium containing 2 μg/ml puromycin. Well-separated antibiotic resistant clone cells were identified and expanded for subsequent experiments.

Western blotting

After three precooled PBS washes, the cells were harvested with lysis buffer (P0013, Beyotime Biotechnology; supplemented with PMSF and phosphorylation inhibitors) and placed on ice for 10 min. Subsequently, the cell lysate was collected into a 1.5 ml tube, followed by centrifugation at 4 °C for 30 min at maximum speed (13,000 rpm). The resulting supernatant was then collected and subjected to BCA quantification (23227, Thermo Fisher). Equal amounts of protein were separated on SDS-polyacrylamide gel electrophoresis gels and transferred onto nitrocellulose filter membranes. The membranes were blocked with 5% milk/TBST (20 mM Tris-HCl, 150 mM NaCl, 0.1% Tween-20, pH 7.6) at room temperature for 1 h and then incubated overnight with the indicated primary antibodies at 4 °C. Proteins were incubated with horseradish peroxidase-conjugated secondary antibodies and visualized in a Chem imaging system. Antibodies used are as follows: Phospho-Akt (Ser473) 4060, Cell Signaling Technology; Phospho-GSK-3β (Ser9), 5558, Cell Signaling Technology; HK2, sc-374091, Santa Cruz Biotechnology; 4EBP2, 2845, Cell Signaling Technology; GAPDH, AC002, ABclonal; G6PD, sc-373886, Santa Cruz Biotechnology; GSK3β, 5676, Cell Signaling Technology; AKT, 9272, Cell Signaling Technology;

PKM, 4053, Cell Signaling Technology; HRP-conjugated Streptavidin, SA00001-0, Proteintech.

RNA extraction and gene expression analysis

Total RNA of cells was extracted using TRIzol (9109, Takara), and translating mRNA was extracted using ribosome extraction kit (EX1380, Solarbio), subsequently reverse transcribed into cDNA using Prime Script RT Master Mix (R036A, Takara). Quantitative polymerase chain reaction was performed using a Bio-Rad system SYBR Green protocol. The results were analyzed using the $2^{-\Delta\Delta Ct}$ method with actin as an internal reference. Oligonucleotide sequences used in RT-PCR shown in the Table S1.

Protein extraction and phosphorylated peptides enrichment for mass spectrometry

Cell lysis buffer, containing 8 M urea, 50 mM Tris-HCl (pH = 7.4), 2% protease cocktail (v/v), 1% Triton X-100, 1 mM $C_3H_7Na_2PO_6$, 1 mM $Na_4O_7P_2$, 1 mM NaF, and 1 mM Na_3VO_4; precipitation buffer, containing acetone (v): absolute ethanol (v): glacial acetic acid (v) = 50: 50: 0.1; resuspension buffer, containing 8 M urea in 100 mM NH_4HCO_3; and click buffer, containing TCEP stock solution (4 mM), $CuSO_4$ stock solution (4 mM), and the tert-butyl 2,2,2-trichloroacetimidate (TBTA) stock solution (100 μM). (Urea, $C_3H_7Na_2PO_6$, $Na_4O_7P_2$, NaF, Na_3VO_4, NH_4HCO_3, TCEP, TBTA and $CuSO_4$ purchased from Sigma).

The enrichment method of phosphorylated peptides by TiO_2 is the same as the published article of our laboratory (48). In briefly, 500 μg protein was reduced with 10 mM DTT (D477470, Aladdin) at room temperature for 45 min, then alkylated with 40 mM iodoacetamide (I131590, Aladdin) at room temperature for 45 min. Trypsin (VA9000, Promega; 1:50 enzyme-protein ratio) were added to samples to digest the protein at 37 °C overnight. Phosphorylation-modified peptides were enriched by TiO_2 (88,303, Thermo Fisher). Phosphorylation-modified peptides were resuspended in 30 μl MS loading buffer (2% ACN, 0.1% FA) for liquid chromatography–tandem mass spectrometry analysis.

Nascent protein label and click chemistry

The labeling method of the nascent proteins is in agreement with the previous report of our laboratory (38). In briefly, HepG2 cells were treated with or without PA (300 μM) for 24 h, then label with AHA. After labeling, the cells were washed with 1 × PBS three times. Cell lysates were collected with lysis buffer, then click reaction was performed at room temperature overnight. Precipitation and resolving proteins were digested into peptide by trypsin. Finally, AHA-labeled peptides were enriched by NeutrAvidin Beads (9204, Thermo Fisher) for mass spectrometry.

Liquid chromatography-tandem mass spectrometry

Peptides were loaded onto silica columns packed in-house (ReproSil Pur C18-AQ, 1.9 μm particle size). Peptides were separated by reversed-phase chromatography using an UltiMate 3000 (Thermo Fisher Scientific), with a binary buffer system of 0.1% formic acid (buffer A) and 80% ACN/0.1% formic (buffer B). Peptides were separated by linear gradients at a flow rate of 300 nl/min and electrosprayed directly into the mass spectrometer by the application of 2.4 kV with a liquid junction union. Ionized peptides were analyzed using a benchtop Orbitrap (Q Exactive PLUS) mass spectrometer (Thermo Fisher Scientific). The mass spectrometer was operated in data-dependent mode. Fragment ions were analyzed with high resolution in the Orbitrap mass analyzer.

MS RAW data processing

Proteins identified and quantified by MaxQuant software using the human or mice database downloaded from UniProt. Adding modification of AHA labeling: AHA replaces methionine and reacts with biotin, resulting in an increase of $C_{12}H_{16}O_2N_6$ (molecular weight: 276.133). Default settings were used, with the addition of "Phospho (STY)" and "AHA labeling" as a variable modification, respectively, and "match between runs" was turned on for all samples analyzed in the same runs.

Cell viability assay (MTT)

HepG2 and 4EBP2-KD cells were seeded in 96-well plates at a density of 4×10^4 per well for 24, 36, 48, 72, and 96 h. Cell viability was measured by the MTT (3-[4,5-dimethylthiazol-2-yl]-2,5 diphenyl tetrazolium bromide) method.

Glucose uptake measurement

4EBP2-KD, 4EBP2-OE, MUTs, and control cells were cultured in high glucose DMEM with or without PA. 4EBP2-KD and control cells were cultured in high glucose DMEM with or without 2-DG for 24 h. Glucose levels in the medium were detected using a Glucose Assay Kit (A154-1-1, Nanjing Jiancheng Bioengineering Institute) according to the manufacturer's instructions. The absorbance values were measured at 570 nm to determine the cellular glucose levels.

Serum AST and ALT detection

Drawing blood from eyeball of mice into a 1.5 ml centrifuge tubes and stand at room temperature for 1 h. Centrifuge at 3000 rpm for 10 min, and the supernatant is serum. The concentration of the serum GPT/ALT and GOT/AST was measured by ALT and AST kit (Nanjing Jiancheng Bioengineering Institute).

Statistical analysis

Data are represented as the mean ± SD. For each chart, the number of independent experiments (n) is given in the legend of the figure. The unpaired two-tailed Student's *t* test was used to compare two independent experimental groups, and the *p*-value was marked in the figures.

Data availability

Source data are provided in this paper. The mass spectrometry proteomics data have been deposited to the

ProteomeXchange Consortium (http://proteomecentral.proteomexchange.org) *via* the iProX partner repository with the dataset identifier PXD041571. Processed data are available as supplementary tables.

Supporting information—This article contains supporting information.

Acknowledgments—The authors thank Ying Zhang at the Instrument Analysis Center of XJTU for mass analysis and Miaomiao Tian at the State key Laboratory of Cancer Biology.

Author contributions—X. H., H. L., and J. L. methodology; X. H., F. Y., Z. Z., Z. W., Z. H., Q. S., T. S., W. L., C. Y., G. Z., and X. P. data curation; X. H., F. Y., Z. Z., Z. W., Z. H., Q. S., T. S., W. L., C. Y., G. Z., and X. P. formal analysis; X. H., H. L., and J. L. writing–review and editing.

Funding and additional information—This work was supported by the Natural Science Foundation of Shandong (No. ZR2022LSW003, H. L.), the National Natural Science Foundation of China (No. 31670781, H. L.), and Xi'an Jiaotong University (No. xzy012020083 and 334100038, H. L.).

Conflict of interest—The authors declare that they have no conflicts of interest with the contents of this article.

Abbreviations—The abbreviations used are: 4EBP2, Eukaryotic translation initiation factor 4E-binding protein 2; AKT, RAC serine/threonine-protein kinase; eIF4E, Eukaryotic translation initiation factor 4E; G6PD, Glucose-6-phosphate 1-dehydrogenase; GLUT4, Solute carrier family 2, facilitated glucose transporter member 4; GSK3B, Glycogen synthase kinase-3 beta; HFD, high-fat diet; HK2, Hexokinase-2; KEGG, Kyoto Encyclopedia of Genes and Genomes; PA, palmitic acid; PKM, Pyruvate kinase PKM; RPTOR, Regulatory-associated protein of mTOR; SEC16A, Protein transport protein Sec16A; sh-, short hairpin; SIK2, Serine/threonine-protein kinase SIK2; T2D, Type 2 diabetes; TBC1D4, TBC1 domain family member 4.

References

1. Houstis, N., Rosen, E. D., and Lander, E. S. (2006) Reactive oxygen species have a causal role in multiple forms of insulin resistance. *Nature* **440**, 944–948
2. Hu, F. B., Manson, J. E., Stampfer, M. J., Colditz, G., Liu, S., Solomon, C. G., *et al.* (2001) Diet, lifestyle, and the risk of type 2 diabetes mellitus in women. *New Engl. J. Med.* **345**, 790–797
3. Zimmet, P., Alberti, K. G., and Shaw, J. (2001) Global and societal implications of the diabetes epidemic. *Nature* **414**, 782–787
4. Lyu, K., Zhang, Y., Zhang, D., Kahn, M., Ter Horst, K. W., Rodrigues, M. R. S., *et al.* (2020) A membrane-bound diacylglycerol species induces PKCε-mediated hepatic insulin resistance. *Cell Metab.* **32**, 654–664.e655
5. Watt, M. J., Miotto, P. M., De Nardo, W., and Montgomery, M. K. (2019) The liver as an endocrine organ-linking NAFLD and insulin resistance. *Endocr. Rev.* **40**, 1367–1393
6. Birkenfeld, A. L., and Shulman, G. I. (2014) Nonalcoholic fatty liver disease, hepatic insulin resistance, and type 2 diabetes. *Hepatology* **59**, 713–723
7. Gao, D., Nong, S., Huang, X., Lu, Y., Zhao, H., Lin, Y., *et al.* (2010) The effects of palmitate on hepatic insulin resistance are mediated by NADPH Oxidase 3-derived reactive oxygen species through JNK and p38MAPK pathways. *J. Biol. Chem.* **285**, 29965–29973
8. Yang, M., Wei, D., Mo, C., Zhang, J., Wang, X., Han, X., *et al.* (2013) Saturated fatty acid palmitate-induced insulin resistance is accompanied with myotube loss and the impaired expression of health benefit myokine genes in C2C12 myotubes. *Lipids Health Dis.* **12**, 104
9. Ishii, M., Maeda, A., Tani, S., and Akagawa, M. (2015) Palmitate induces insulin resistance in human HepG2 hepatocytes by enhancing ubiquitination and proteasomal degradation of key insulin signaling molecules. *Arch. Biochem. Biophys.* **566**, 26–35
10. Shimobayashi, M., and Hall, M. N. (2014) Making new contacts: the mTOR network in metabolism and signalling crosstalk. *Nat. Rev. Mol. Cell Biol.* **15**, 155–162
11. Efeyan, A., Comb, W. C., and Sabatini, D. M. (2015) Nutrient-sensing mechanisms and pathways. *Nature* **517**, 302–310
12. Guertin, D. A., and Sabatini, D. M. (2007) Defining the role of mTOR in cancer. *Cancer Cell* **12**, 9–22
13. Fingar, D. C., Salama, S., Tsou, C., Harlow, E., and Blenis, J. (2002) Mammalian cell size is controlled by mTOR and its downstream targets S6K1 and 4EBP1/eIF4E. *Genes Dev.* **16**, 1472–1487
14. Tsukiyama-Kohara, K., Poulin, F., Kohara, M., DeMaria, C. T., Cheng, A., Wu, Z., *et al.* (2001) Adipose tissue reduction in mice lacking the translational inhibitor 4E-BP1. *Nat. Med.* **7**, 1128–1132
15. Hu, C., Pang, S., Kong, X., Velleca, M., and Lawrence, J. C., Jr. (1994) Molecular cloning and tissue distribution of PHAS-I, an intracellular target for insulin and growth factors. *Proc. Natl. Acad. Sci. U. S. A.* **91**, 3730–3734
16. Poulin, F., Gingras, A. C., Olsen, H., Chevalier, S., and Sonenberg, N. (1998) 4E-BP3, a new member of the eukaryotic initiation factor 4E-binding protein family. *J. Biol. Chem.* **273**, 14002–14007
17. Teleman, A. A., Chen, Y. W., and Cohen, S. M. (2005) 4E-BP functions as a metabolic brake used under stress conditions but not during normal growth. *Genes Dev.* **19**, 1844–1848
18. Yu, X. X., Pandey, S. K., Booten, S. L., Murray, S. F., Monia, B. P., and Bhanot, S. (2008) Reduced adiposity and improved insulin sensitivity in obese mice with antisense suppression of 4E-BP2 expression. *Am. J. Physiol. Endocrinol. Metab.* **294**, E530–539
19. Caon, I., Parnigoni, A., Viola, M., Karousou, E., Passi, A., and Vigetti, D. (2021) Cell energy metabolism and hyaluronan synthesis. *J. Histochem. Cytochem.* **69**, 35–47
20. Teng, Y. H., Aquino, R. S., and Park, P. W. (2012) Molecular functions of syndecan-1 in disease. *Matrix Biol.* **31**, 3–16
21. Merline, R., Moreth, K., Beckmann, J., Nastase, M. V., Zeng-Brouwers, J., Tralhão, J. G., *et al.* (2011) Signaling by the matrix proteoglycan decorin controls inflammation and cancer through PDCD4 and MicroRNA-21. *Sci. Signal.* **4**, ra75
22. Miinea, C. P., Sano, H., Kane, S., Sano, E., Fukuda, M., Peränen, J., *et al.* (2005) AS160, the Akt substrate regulating GLUT4 translocation, has a functional Rab GTPase-activating protein domain. *Biochem. J.* **391**, 87–93
23. Baus, D., Heermeier, K., De Hoop, M., Metz-Weidmann, C., Gassenhuber, J., Dittrich, W., *et al.* (2008) Identification of a novel AS160 splice variant that regulates GLUT4 translocation and glucose-uptake in rat muscle cells. *Cell Signal.* **20**, 2237–2246
24. Chen, Y., Wang, Y., Zhang, J., Deng, Y., Jiang, L., Song, E., *et al.* (2012) Rab10 and myosin-Va mediate insulin-stimulated GLUT4 storage vesicle translocation in adipocytes. *J. Cell Biol.* **198**, 545–560
25. Feng, Y., Hartig, S. M., Bechill, J. E., Blanchard, E. G., Caudell, E., and Corey, S. J. (2010) The Cdc42-interacting protein-4 (CIP4) gene knockout mouse reveals delayed and decreased endocytosis. *J. Biol. Chem.* **285**, 4348–4354
26. Coffey, S., Costacou, T., Orchard, T., and Erkan, E. (2015) Akt links insulin signaling to albumin endocytosis in proximal tubule epithelial cells. *PLoS One* **10**, e0140417
27. Vind, B. F., Pehmøller, C., Treebak, J. T., Birk, J. B., Hey-Mogensen, M., Beck-Nielsen, H., *et al.* (2011) Impaired insulin-induced site-specific phosphorylation of TBC1 domain family, member 4 (TBC1D4) in skeletal muscle of type 2 diabetes patients is restored by endurance exercise-training. *Diabetologia* **54**, 157–167
28. Bruno, J., Brumfield, A., Chaudhary, N., Iaea, D., and McGraw, T. E. (2016) SEC16A is a RAB10 effector required for insulin-stimulated GLUT4 trafficking in adipocytes. *J. Cell Biol.* **214**, 61–76

29. Screaton, R. A., Conkright, M. D., Katoh, Y., Best, J. L., Canettieri, G., Jeffries, S., *et al.* (2004) The CREB coactivator TORC2 functions as a calcium- and cAMP-sensitive coincidence detector. *Cell* **119**, 61–74
30. Lee, C. W., Yang, F. C., Chang, H. Y., Chou, H., Tan, B. C., and Lee, S. C. (2014) Interaction between salt-inducible kinase 2 and protein phosphatase 2A regulates the activity of calcium/calmodulin-dependent protein kinase I and protein phosphatase methylesterase-1. *J. Biol. Chem.* **289**, 21108–21119
31. Geng, J., Sun, X., Wang, P., Zhang, S., Wang, X., Wu, H., *et al.* (2015) Kinases Mst1 and Mst2 positively regulate phagocytic induction of reactive oxygen species and bactericidal activity. *Nat. Immunol.* **16**, 1142–1152
32. Hauge, C., Antal, T. L., Hirschberg, D., Doehn, U., Thorup, K., Idrissova, L., *et al.* (2007) Mechanism for activation of the growth factor-activated AGC kinases by turn motif phosphorylation. *EMBO J.* **26**, 2251–2261
33. Yang, T. T., Xiong, Q., Graef, I. A., Crabtree, G. R., and Chow, C. W. (2005) Recruitment of the extracellular signal-regulated kinase/ribosomal S6 kinase signaling pathway to the NFATc4 transcription activation complex. *Mol. Cell Biol.* **25**, 907–920
34. Tanaka, S., Hikita, H., Tatsumi, T., Sakamori, R., Nozaki, Y., Sakane, S., *et al.* (2016) Rubicon inhibits autophagy and accelerates hepatocyte apoptosis and lipid accumulation in nonalcoholic fatty liver disease in mice. *Hepatology* **64**, 1994–2014
35. Lukhele, S., Bah, A., Lin, H., Sonenberg, N., and Forman-Kay, J. D. (2013) *Interaction of the Eukaryotic Initiation Factor 4E with 4E-BP2 at a Dynamic Bipartite Interface*, 1993. 21. Structure, London, England: 2186–2196
36. Bah, A., Vernon, R. M., Siddiqui, Z., Krzeminski, M., Muhandiram, R., Zhao, C., *et al.* (2015) Folding of an intrinsically disordered protein by phosphorylation as a regulatory switch. *Nature* **519**, 106–109
37. Hou, Z., Han, X., Wang, Z., Ghazanfar, S., Yang, J., and Liu, H. (2021) A terminal alkyne and disulfide functionalized agarose resin specifically enriches azidohomoalanine labeled nascent proteins. *J. Chromatogr. B, Anal. Tech. Biomed. Life Sci.* **1165**, 122527
38. Zhang, Z., Zeng, M., Han, X., Hou, Z., Wang, Z., Su, T., *et al.* (2022) A nascent protein labeling strategy disclosed mitochondrial proteomic responses in punicalagin intervened insulin resistance of HepG2 cells. *Food Funct.* **13**, 1180–1191
39. Herzig, S., and Shaw, R. J. (2018) AMPK: guardian of metabolism and mitochondrial homeostasis. *Nat. Rev. Mol. Cell Biol.* **19**, 121–135
40. Palomer, X., Pizarro-Delgado, J., Barroso, E., and Vázquez-Carrera, M. (2018) Palmitic and oleic acid: the yin and yang of fatty acids in type 2 diabetes mellitus. *Trends Endocrinol. Metab.* **29**, 178–190
41. Marcotrigiano, J., Gingras, A. C., Sonenberg, N., and Burley, S. K. (1999) Cap-dependent translation initiation in eukaryotes is regulated by a molecular mimic of eIF4G. *Mol. Cell* **3**, 707–716
42. Tait, S., Dutta, K., Cowburn, D., Warwicker, J., Doig, A. J., and McCarthy, J. E. (2010) Local control of a disorder-order transition in 4E-BP1 underpins regulation of translation *via* eIF4E. *Proc. Natl. Acad. Sci. U. S. A.* **107**, 17627–17632
43. Sarbassov, D. D., Guertin, D. A., Ali, S. M., and Sabatini, D. M. (2005) Phosphorylation and regulation of Akt/PKB by the rictor-mTOR complex. *Science (New York, N.Y.)* **307**, 1098–1101
44. Yang, J., Cron, P., Thompson, V., Good, V. M., Hess, D., Hemmings, B. A., *et al.* (2002) Molecular mechanism for the regulation of protein kinase B/Akt by hydrophobic motif phosphorylation. *Mol. Cell* **9**, 1227–1240
45. Demetriades, C., Doumpas, N., and Teleman, A. A. (2014) Regulation of TORC1 in response to amino acid starvation *via* lysosomal recruitment of TSC2. *Cell* **156**, 786–799
46. Gingras, A. C., Raught, B., and Sonenberg, N. (2004) mTOR signaling to translation. *Curr. Top. Microbiol. Immunol.* **279**, 169–197
47. Liu, X., Cao, K., Lv, W., Feng, Z., Liu, J., Gao, J., *et al.* (2019) Punicalagin attenuates endothelial dysfunction by activating FoxO1, a pivotal regulating switch of mitochondrial biogenesis. *Free Radic. Biol. Med.* **135**, 251–260
48. Wang, Z., Lei, P., Li, Z., Han, X., Yang, F., Su, T., *et al.* (2022) Proteomic and phosphoproteomic analyses reveal the oncogenic role of PTK7-NDRG1 Axis in non-small-cell lung cancer cell resistance to AZD9291. *ACS Chem. Biol.* **17**, 2849–2862